ELSEVIER

Surface Science 500 (2002) 218–241

SURFACE SCIENCE

www.elsevier.com/locate/susc

Carbon nanotubes: opportunities and challenges

Hongjie Dai *

Department of Chemistry, Stanford University, Stanford, CA 94305, USA

Received 14 August 2000; accepted for publication 11 July 2001

Abstract

Carbon nanotubes are graphene sheets rolled-up into cylinders with diameters as small as one nanometer. Extensive work carried out worldwide in recent years has revealed the intriguing electrical and mechanical properties of these novel molecular scale wires. It is now well established that carbon nanotubes are ideal model systems for studying the physics in one-dimensional solids and have significant potential as building blocks for various practical nanoscale devices. Nanotubes have been shown to be useful for miniaturized electronic, mechanical, electromechanical, chemical and scanning probe devices and materials for macroscopic composites. Progress in nanotube growth has facilitated the fundamental study and applications of nanotubes. Gaining control over challenging nanotube growth issues is critical to the future advancement of nanotube science and technology, and is being actively pursued by researchers.

Keywords: Carbon; Chemical vapor deposition; Electrical transport measurements; Quantum effects; Chemisorption

1. Introduction

A new form of carbon, buckministerfullerene C_{60} was discovered in 1985 by a team headed by Smalley, Kroto and coworkers [1], and led to the Nobel Prize in chemistry in 1997. C_{60} is a soccer ball-like molecule made of pure carbon atoms bonded in hexagon and pentagon configurations. Besides diamond, graphite and C_{60}, quasi one-dimensional nanotube is another form of carbon first reported by Iijima in 1991 when he discovered multi-walled carbon nanotubes (MWNT) in carbon-soot made by an arc-discharge method [2]. About two years later, he made the observation of single-walled nanotubes (SWNTs) [3]. Since then, nanotubes have captured the attention of researchers worldwide. A significant amount of work has been done in the past decade to reveal the unique structural, electrical, mechanical, electromechanical and chemical properties of carbon nanotubes and to explore what might be the key applications of these novel materials.

A SWNT is a graphene sheet (Fig. 1) rolled-over into a cylinder with typical diameter on the order of 1.4 nm (Fig. 3a–d), similar to that of a C_{60} buckyball. A MWNT consists of concentric cylinders with an interlayer spacing of 3.4 Å and a diameter typically on the order of 10–20 nm (Fig. 2a–c). The lengths of the two types of tubes can be up to hundreds of microns or even centimeters. A SWNT is a molecular scale wire that has two key structural parameters. By folding a graphene sheet into a

* Fax: +1-650-725-0259.
E-mail address: hdai1@stanford.edu (H. Dai).

0039-6028/01/$ - see front matter
PII: S0039-6028(01)01558-8

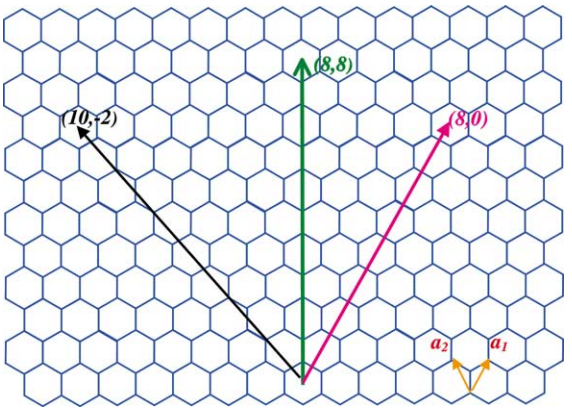

Fig. 1. Schematic honeycomb structure of a graphene sheet. Carbon atoms are at the vertices. SWNTs can be formed by folding the sheet along lattice vectors. The two basis vectors $\boldsymbol{a}_1$ and $\boldsymbol{a}_2$, and several examples of the lattice vectors are shown.

cylinder so that the beginning and end of a (m,n) lattice vector in the graphene plane join together (Fig. 1), one obtains an (m,n) nanotube. The (m,n) indices determine the diameter of the nanotube, and also the so-called 'chirality'. (m,m) tubes are 'arm-chair' tubes, since the atoms around the circumference are in an arm-chair pattern (Fig. 3a). $(m,0)$ nanotubes are termed 'zigzag' in view of the atomic configuration along the circumference (Fig. 3b and c). The other types of nanotubes are chiral, with the rows of hexagons spiraling along the nanotube axes (Fig. 3d).

In terms of mechanical properties, nanotubes are among the strongest and most resilient materials known to exist in nature. A nanotube has a Young's modulus of 1.2 TPa and tensile strength about a hundred times higher than steel and can tolerate large strains before mechanical failure [4]. The electrical properties of nanotubes depend sensitively on the (m,n) indices and therefore on the diameter and chirality. A SWNT can be either a metal, semiconductor or small-gap semiconductor depending on the (m,n) structural parameters [5]. For a graphene sheet, the conduction and valence bands touch each other at the six corner points of the first Broulloin zone. These states are filled with electrons that have the highest energy (Fermi's energy). A graphene sheet is therefore semimetallic with a zero band gap. The electronic states of an infinitely long nanotube are parallel lines in $\mathbf{k}$ space, continuous along the tube axis and quantized along the circumference (Fig. 3a–d). For (m,m) arm-chair tubes, there are always states crossing the corner points of the first Brillouin zone (Fig. 3a), suggesting that arm-chair tubes should always be metallic. For (m,n) nanotubes with $m-n \neq 3\times$ integer, the electronic states (lines) miss the corner points (Fig. 3c and d) and the nanotubes are semiconducting. The energy gap scales with the tube diameter as $1/d$ and is on the order of 0.5 eV for a SWNT with typical diameter $d = 1.4$ nm. For $m-n = 3\times$ integer, certain electronic states of the nanotube land on the corner points of the first Broulloin zone (Fig. 3b). These types of tubes would be semimetals but become small-gap semiconductors (band gap scales with $1/d^2 \sim 10$ meV for $d \sim 1.4$ nm) due to a curvature induced orbital rehybridization effect [6]. The extreme sensitivity of electronic property on structural parameters is unique for carbon nanotubes. This uniqueness leads to rich physical phenomena in nanotube systems, and poses a significant challenge to chemical synthesis in terms of controlling the nanotube diameter and chirality.

The intriguing properties of carbon nanotubes have led to an explosion of research efforts worldwide [7]. Understanding these properties and exploring their potential applications have been a main driving force in this area. Theoretical and experimental work has been focusing on the relationship between nanotube atomic structures and electronic structures, transport properties, electron–electron and electron–phonon interaction effects. Extensive effort has been made to investigate the mechanical properties of nanotubes, including their Young's modulus, tensile strength, failure processes and mechanisms. It has also been an important fundamental question regarding how mechanical deformation in a nanotube affects its electrical properties.

Thus far, nanotubes have been utilized individually or as an ensemble to build functional device prototypes, as has been demonstrated by many research groups. Ensembles of nanotubes have been used for field emission based flat-panel displays, composite materials with improved mechanical properties and electromechanical actuators. Bulk

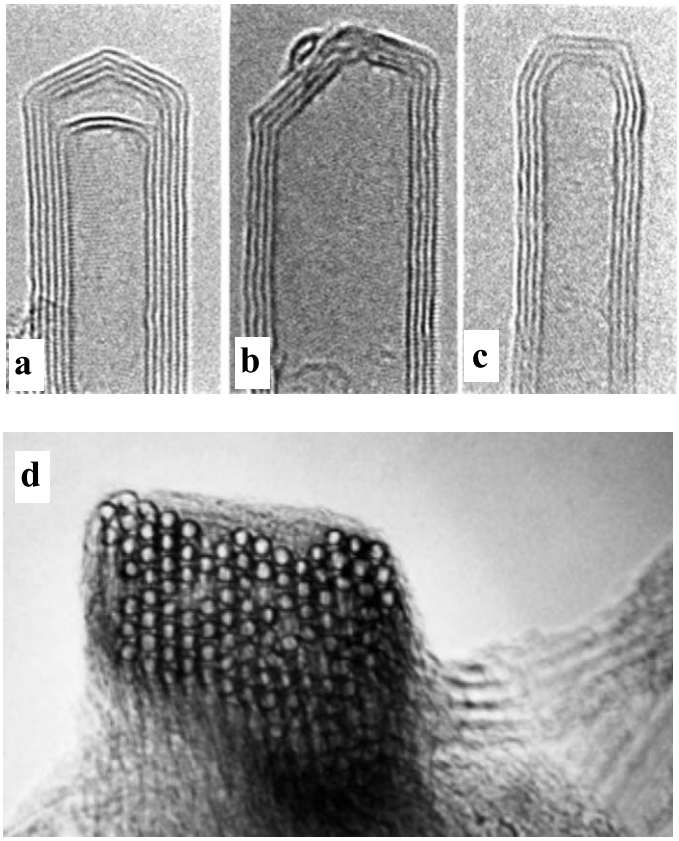

Fig. 2. Viewing the invisible: carbon nanotubes imaged by transmission electron microscopy (TEM). TEM is a technique used in the discovery of both MWNTs and SWNTs. (a–c) TEM images of MWNTs with closed caps (courtesy of S. Iijima). The parallel lines are the cross-sections of the sidewalls of concentric cylinders. Diameters of MWNTs are typically on the order of 10–20 nm. (d) TEM image of the cross-section of a bundle of SWNTs (courtesy of R. Smalley). Each circle represents the cross-section of a SWNT with diameter ~1.4 nm.

quantities of nanotubes have also been suggested as high-capacity hydrogen storage media. Individual nanotubes have been used for field emission sources, tips for scanning probe microscopy, nanotweezers and chemical sensors. Nanotubes are also promising as the central elements for future miniaturized electronic devices.

The success in nanotube growth has led to the wide availability of nanotube materials, which is a main catalyst behind the recent leaps-and-bounds in basis physics studies and applications of nanotubes [7]. The full potential of nanotubes for applications will not be realized until the growth of nanotubes can be further optimized and controlled. Real-world applications of nanotubes require either large quantities of bulk materials or device integration in a scale-up fashion. For applications such as composites and hydrogen storage, it is desired to obtain high quality nanotubes at the kilogram or ton level using growth methods that are simple, efficient and inexpensive. For devices such as nanotube based electronics, scale-up will unavoidably rely on self-assembly techniques or controlled growth strategies on surfaces combined with microfabrication techniques. Significant work has been carried out to tackle these issues. Nevertheless, many challenges remain in the nanotube growth area. An efficient growth approach to

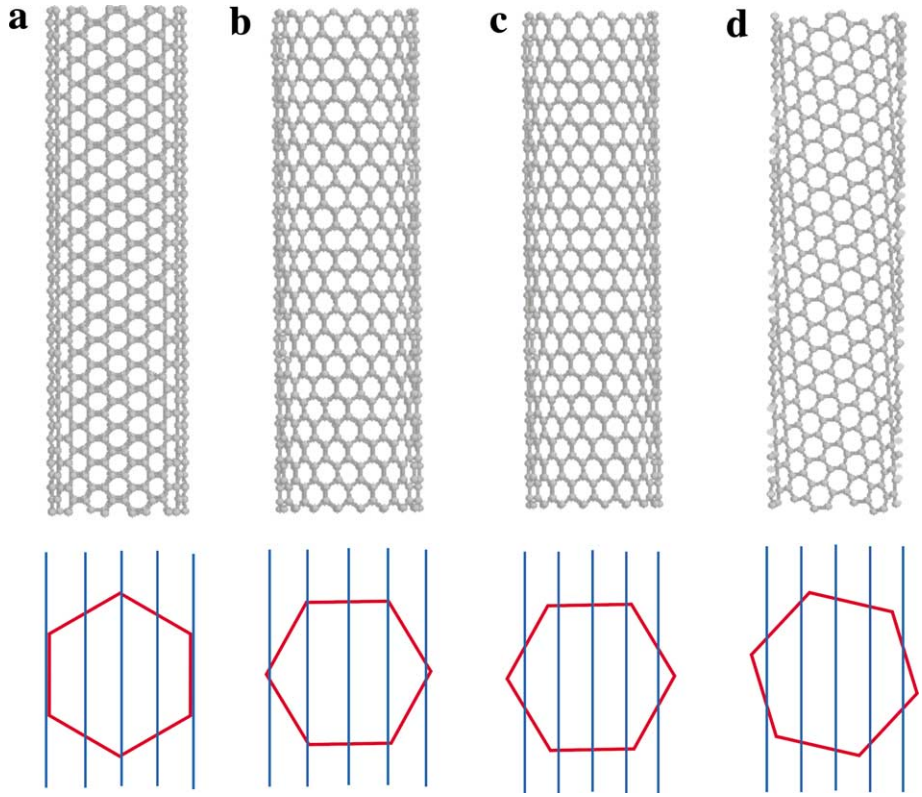

Fig. 3. Schematic structures of SWNTs and how they determine the electronic properties of the nanotubes. (a) A (10,10) arm-chair nanotube. Bottom panel: the hexagon represents the first Broulloin zone of a graphene sheet in reciprocal space. The vertical lines represent the electronic states of the nanotube. The center-line crosses two corners of the hexagon, resulting in a metallic nanotube. (b) A (12, 0) zigzag nanotube. The electronic states cross the hexagon corners, but a small band gap can develop due to the curvature of the nanotube. (c) The (14, 0) zigzag tube is semiconducting because the states on the vertical lines miss the corner points of the hexagon. (d) A (7, 16) tube is semiconducting. This figure illustrates the extreme sensitivity of nanotube electronic structures to the diameter and chirality of nanotubes.

structurally perfect nanotubes at large scales is not yet at hand. Growing defect-free nanotubes continuously to macroscopic lengths is still difficult. Also, it is desired to gain exquisite control over nanotube growth on surfaces and to obtain large-scale ordered nanowire structures. Finally, there is a seemingly formidable task of controlling the chirality of SWNTs during growth.

2. Nanotube growth

Arc-discharge and laser ablation methods for the growth of nanotubes have been actively pursued in the past 10 years. In 1992, a breakthrough in MWNT growth by arc-discharge was first by Ebbesen and Ajayan who achieved growth and purification of high quality MWNTs at the gram level [8]. The synthesized MWNTs have lengths on the order of 10 μm and diameters in the range of 5–30 nm. The nanotubes are typically bound together by strong van der Waals interactions and form tight bundles. For the growth of single-walled tubes, a metal catalyst is needed in the arc-discharge system. The first success in producing substantial amounts of SWNTs by arc-discharge was achieved by Bethune and coworkers in 1993 [9]. The growth of high quality SWNTs at the 1–10 g scale was achieved by Smalley and coworkers using a laser ablation (laser oven) method [10]. The

produced SWNTs are mostly in the form of ropes consisting of tens of individual nanotubes close packed into hexagonal crystals via van der Waals interactions (Fig. 2d). The optimization of SWNT growth by arc-discharge was achieved by Journet and coworkers using a carbon anode containing 1.0 at.% of yttrium and 4.2 at.% of nickel as catalysts [11].

Another method for producing solid state carbon materials is chemical vapor deposition (CVD) of hydrocarbon gases. CVD methods have been successful in making carbon fiber, filament and nanotube materials for more than 20 years [12–16]. The growth process involves heating a catalyst material to high temperatures (500–1000 °C) in a tube furnace, and flowing a hydrocarbon gas through the tube reactor over a period of time. The catalytic species are typically transition-metal nanoparticles that are formed on a support material such as porous aluminum oxide (alumina) materials with large surface areas. The general nanotube growth mechanism in a CVD process involves the dissociation of hydrocarbon molecules catalyzed by the transition metal, and dissolution and saturation of carbon atoms in the metal nanoparticle. The precipitation of carbon from the saturated metal particle leads to the formation of tubular carbon solids in an sp^2 structure. Tubule formation is favored over other forms of carbon such as graphitic sheets with open edges. This is due to that a tube contains no dangling bonds and therefore is in a low energy form. For MWNT growth, most of the CVD methods employ ethylene or acetylene as the carbon feedstock and the growth temperature is typically in the range of 550–750 °C. Iron, nickel or cobalt nanoparticles are often used as catalysts. The rationale for choosing these metals as catalysts for CVD growth of nanotubes lies in the phase diagrams for the metals and carbon. At high temperatures, carbon has a finite solubility in these metals, which leads to the formation of metal–carbon solid state solutions and therefore to the aforementioned growth mechanism.

CVD methods have great potential for scaled-up nanotube materials synthesis. Multi-walled nanotubes have already been produced commercially on the kilogram to ton level. Nevertheless, these MWNTs tend to contain high densities of defects such as pentagons and heptagons on the sidewalls of the nanotubes. The success of nearly defect-free single-walled carbon nanotube growth by CVD is relatively recent.

Our group has found that by using methane as carbon feedstock, reaction temperatures in the range of 850–1000 °C and alumina supported catalyst materials, one can grow high quality SWNT materials by CVD [17–20]. High growth temperatures favor the formation of SWNTs that have small diameters and thus high strain energies, and allow for nearly defect-free tube structures. Methane is the most stable hydrocarbon against self-decomposition at high temperatures, and the catalytic decomposition of methane by the transition-metal catalyst particles is the dominant process in SWNT growth. Highly porous catalysts with strong metal–support interactions and high surface areas produce SWNTs with better quality at larger quantities. Strong metal–support interaction means high metal dispersion and thus a high density of catalytic sites on the support. The strong interaction can prevent metal species from aggregating and forming unwanted large particles that could yield to graphitic particles or defective multi-walled tubular structures in CVD. Large surface area and a highly porous structure of the catalyst increase the yield of SWNTs, because of a high density of catalytic sites owing to the former and rapid diffusion and efficient supply of carbon feedstock to the catalytic sites owing to the latter.

Liu and coworkers made significant progress recently in obtaining an excellent catalyst for methane CVD growth of SWNTs [21]. The catalyst preparation involved supercritical drying at high pressure and temperature conditions. The catalyst exhibited ultra-high surface area and porous structure as preserved by the supercritical drying condition under which destructive capillary forces are non-existent. The catalyst yielded abundant SWNTs in CVD. In general, understanding the chemistry involved in catalyst preparation and nanotube growth should lead to further breakthroughs towards scale-up of the growth of perfect SWNT materials.

CVD of methane for the growth of bulk amounts of SWNTs has been investigated by Rao and

coworkers using catalysts based on mixed oxide spinels [22]. Good quality and quantity nanotubes were obtained with nanoparticles of a Fe–Co alloy. Colomer and coworkers recently reported the growth of bulk quantities of SWNTs by CVD of methane using a cobalt catalyst supported on magnesium oxide materials [23].

It has been demonstrated that catalytic growth of SWNTs can be achieved by CVD of several types of hydrocarbons and certain carbon-containing molecules. A CVD approach to SWNTs was developed by Smalley and coworkers who used supported catalysts, ethylene as carbon feedstock and growth temperature around 800 °C [24]. In this case, low partial-pressure ethylene was employed in order to reduce amorphous carbon formation due to the self-decomposition of ethylene at the high growth temperature.

Catalyst particles can be generated from the gas phase in situ for the growth of SWNTs by CVD. Cheng and coworkers reported a method that employs benzene as the carbon feedstock, hydrogen as the carrier gas, and ferrocene as the catalyst precursor for SWNT growth [25]. In this method, ferrocene is vaporized and carried into a reaction tube by benzene and hydrogen gases. The reaction tube is heated at 1100–1200 °C. The vaporized ferrocene decomposes in the reactor, which leads to the formation of iron particles that can catalyze the growth of SWNTs. More recently, the Smalley group developed a gas phase catalytic process to grow bulk quantities of SWNTs [26]. Carbon monoxide (CO) is used as the carbon feedstock and the growth temperature is in the range of 800–1200 °C. Catalytic particles for SWNT growth are generated in situ by thermal decomposition of iron pentacarbonyl in a reactor heated to the growth temperature. CO provides the carbon feedstock for the growth of nanotubes off the iron catalyst particles.

CVD and gas phase catalytic growth of nanotubes have been actively pursued in recent years because of their significant potential for materials scale-up. With continued effort in this area, it is expected that large quantities (up to tons) of high quality nanotube materials can be produced in the near future.

3. Controlled nanotube growth by chemical vapor deposition

With arc-discharge or laser ablation techniques, only tangled nanotubes mixed randomly with various impurities are obtainable. Recent research activities in CVD nanotube growth have also been sparked by the idea that aligned and ordered nanotube structures can be grown on surfaces with control [17]. Xie et al. have grown aligned MWNTs out of the pores of mesoporous silica [27,28] by a CVD approach. The catalyst used is iron oxide particles embedded in the pores of silica. The carbon feedstock is 9% acetylene in nitrogen at an overall 180 Torr pressure, and the growth temperature is 600 °C. Remarkably, nanotubes with lengths up to milimeters are made (Fig. 4a) [28]. Ren and coworkers have been able to grow large-diameter MWNTs forming oriented 'forests' (Fig. 4b) on glass substrates [29]. Plasma-assisted CVD at 660 °C is used in this work with nickel as the catalyst, and acetylene as the carbon feedstock. Fan and coworkers have obtained ordered MWNT structures by CVD on catalytically patterned substrates [30–32]. MWNTs self-assemble into aligned structures during CVD growth. Squared iron patterns on porous silicon substrates are employed for the growth. Regularly positioned arrays of nanotube towers are grown on the substrate (Fig. 4c and d). The nanotube towers exhibit very sharp edges and corners with no nanotubes branching away from the blocks. The MWNTs within each block are well aligned along the direction perpendicular to the substrate surface [30]. The mechanism of nanotube self-orientation involves the nanotube base-growth mode substrates [30]. During CVD growth, the outmost walls of the nanotubes interact with their neighbors via van der Waals forces to form a rigid bundle, which allows the nanotubes to self-orient and grow perpendicular to the substrate.

It is challenging to grow SWNTs into structures with well controlled orientations. Nevertheless, suspended SWNT networks with directionality on substrates containing lithographically patterned silicon pillars have been grown. Contact printing is used to transfer catalyst materials onto the tops of

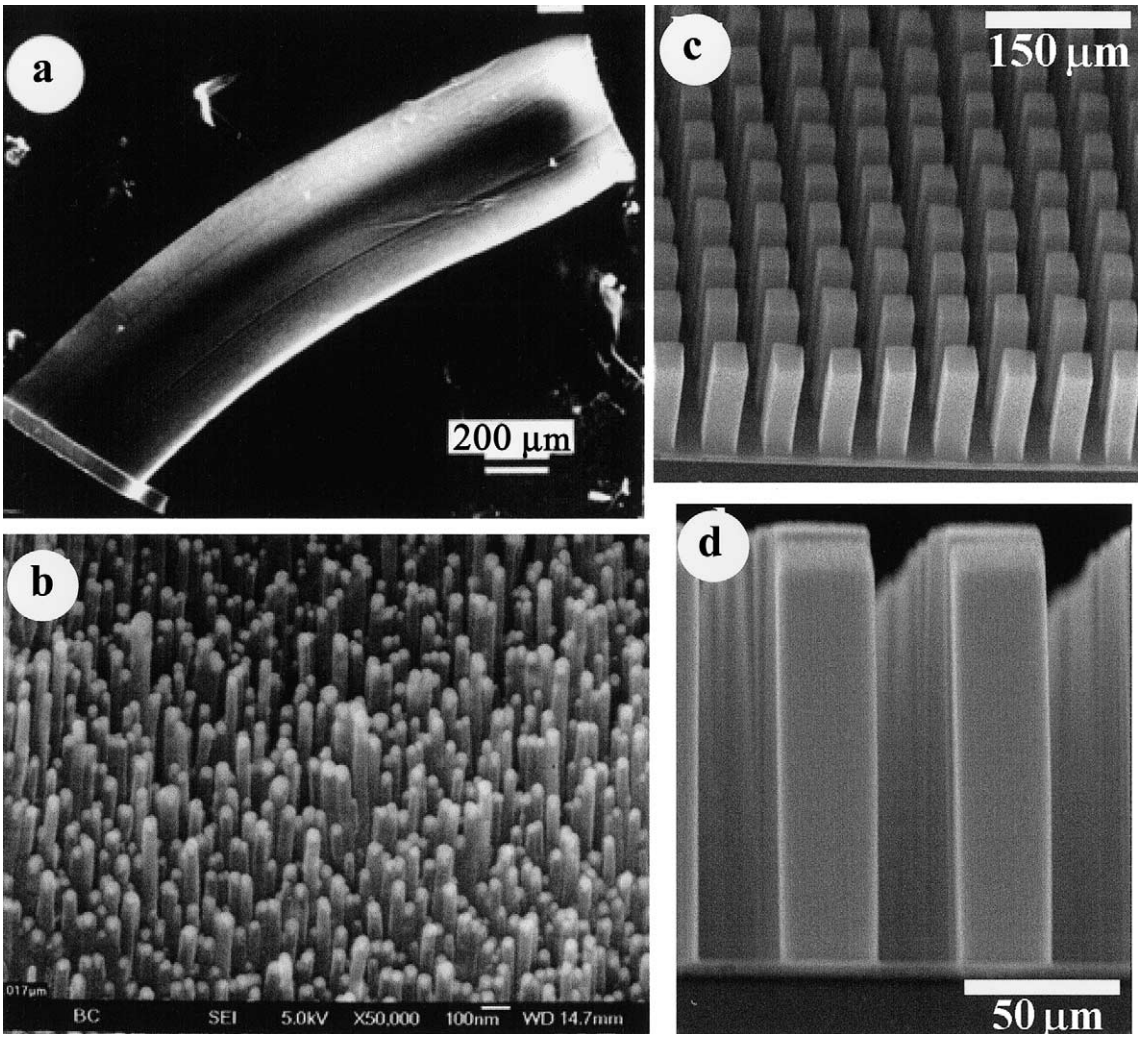

Fig. 4. Aligned MWNT structures grown by CVD methods on various substrates. These structures illustrate that ordered nanotubes can be obtained by direct chemical synthesis approaches. (a) An ultra-long nanotube bundle (courtesy of Dr. S. Xie). The slightly curved cylindrical object (diameter ~600 μm, length ~2 mm) is a large bundle of many aligned nanotubes along the length of the cylinder. (b) An oriented MWNT forest grown on a glass substrate (courtesy of Dr. Z. Ren). Each rod-like object in the image is a MWNT with diameter on the order of tens of nanometers. The nanotubes are grown on a glass substrate (not shown in the image) and are oriented perpendicular to the substrate. (c) SEM image of self-oriented MWNT arrays (Fan et al.). Each tower-like structure is formed by many closely packed MWNT. Nanotubes in each tower are oriented perpendicular to the substrate. (d) Microscopic ''twin towers'': SEM image of the side view of the towers.

pillars selectively. CVD of methane using the substrates leads to suspended SWNTs forming nearly ordered networks with the nanotube orientations directed by the pattern of the pillars (Fig. 5) [33,34]. Nanotubes are nucleated on the tops of the pillars and lengthen from there as they grow. The methane flow keeps the nanotubes floating and waving in the 'wind' since the flow velocity near the bottom surface is substantially lower than that at the level of the tower tops. This prevents

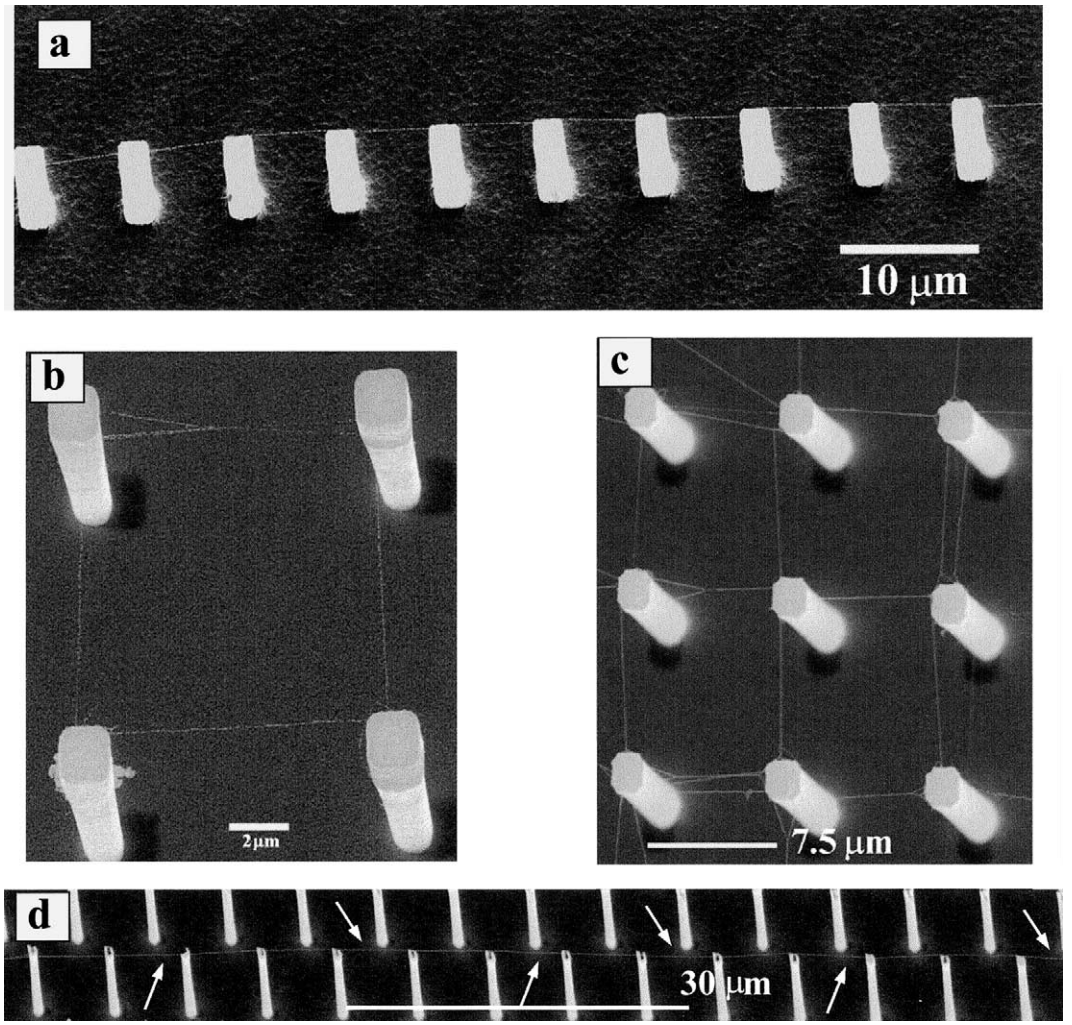

Fig. 5. 'Self-directed' growth of suspended SWNTs. (a) SEM image of suspended SWNT 'power-line' grown on a row of silicon pillars (bright post-like objects). The line-like structures bridging the posts are SWNTs. (b) A square of suspended SWNT. (c) A square network of suspended SWNTs. (d) A long SWNT bridging many silicon pillars. These results demonstrate that ordered networks of SWNTs can be obtained by self-assembled nanotube growth, which could be utilized for building interesting circuits/devices of nanotubes.

the SWNTs from being caught by the bottom surface. The nearby towers on the other hand provide fixation points for the growing tubes. If the waving SWNTs contact adjacent towers, the tube-tower van der Waals interactions will catch the nanotubes and hold them aloft. Single-wall nanotubes that are as long as 0.2 mm (200 μm) in length have been grown (Fig. 5d) [34].

An important aspect of nanotube growth is related to carbon nanotubes as advanced probe tips for scanning probe microscopy (SPM). Nanotubes present ideal characteristics for enhancing the capabilities of SPM in imaging, manipulation and nanolithography. This is owing to the sharpness of the nanotubes, their high aspect ratios, high mechanical stiffness and resilience, and tunable chemical characteristics [35–43]. Nanotube AFM tips have been previously obtained by attaching MWNTs [35,36] and SWNT bundles [40] to the sides of silicon pyramidal tips. Recently, CVD

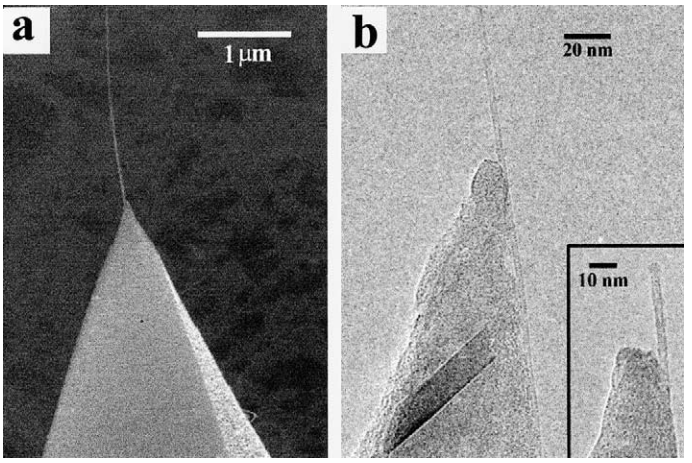

Fig. 6. SWNTs as tips for atomic force microscopy. Nanotubes can be directly grown on conventional silicon tips by CVD methods. (a) SEM image of a SWNT grown on a conical Si tip. The line-like structure extending out of the Si tip is a nanotube. (b) TEM image of the nanotube tip before and after (inset) the length of the tube is reduced by discharging. The nanotube tip has a diameter of only ~2 nm, highly desirable for high resolution AFM imaging.

methods were used to directly grow MWNTs [41] and SWNTs [42,43] on silicon tips for the synthesis of nanotube AFM tips. Hafner and Lieber grew MWNT probe tips by the CVD of ethylene on silicon probes containing straight holes with catalyst particles deposited at the bottom [41]. They also obtained SWNT probe tips by CVD with silicon pyramidal tips with catalyst particles deposited on the sides of the silicon tips [42]. Our group has grown SWNT tips using dip coating of silicon pyramids in a liquid phase catalyst [33] followed by CVD of methane [43]. In the case of SWNT tips, the orientations of the nanotubes (individual or small bundles, Fig. 6a and b) are maintained by van der Waals interactions between the nanotube and the pyramid surface. The SWNTs extending from silicon pyramid tips typically range 1–20 μm in length beyond the pyramid tip. The nanotubes are shortened to ~30–100 nm in order to obtain rigid AFM probe tips (e.g., Fig. 6b inset) needed for probing [43].

Wong and coworkers obtained chemically functionalized carbon nanotube probe tips by opening the ends of nanotubes and terminate the ends with oxygen containing groups such as –COOH [36]. Nanotube tips with a variety of functional chemical groups at the ends were obtained. Biological molecules were also attached to the ends of nanotube tips by reacting functional groups at the ends of nanotubes with reactive sites on the biomolecules. These nanotube tips were shown to be not only superior in obtaining high lateral resolution in real-space imaging of surfaces and biological molecules, but also promising for measuring chemical forces between small numbers of molecules and mapping out chemical characteristics of surfaces with 1 nm spatial resolution [36]. Nanotube tips were also ideal for nanoscale surface modification and scanning probe lithography [38,43]. MWNT tips were used to fabricate ~10–20 nm wide oxide lines on silicon surfaces. SWNT tips were used to fabricate oxide structures with feature size below 10 nm [43]. Nanotubes tips had an overall longer life-time in both imaging and nanofabrication processes than silicon tips owing to their excellent mechanical strength and resilience.

4. Probing the properties of individual nanotube molecular wires

4.1. Correlation between atomic structures and electronic properties

Nanotubes are ideal for studying structure–property relations for atomically well-defined

one-dimensional materials. Elegant work has been carried out by Lieber and Dekker's group who used scanning tunneling microscopy (STM) to directly reveal the real-space atomic structures of SWNTs with various chiralities. At the same time, the electronic structures of the nanotubes are probed and then correlated with the structural properties [44,45]. In STM, electrons tunnel between a sharp metal tip biased against a conducting substrate (in this case nanotubes deposited on metal surfaces). The tunnel current is proportional to the local electronic density of states of the nanotube. Real-space images reflecting the atomic corrugation of the nanotubes can be obtained (Fig. 7a). Local electronic density of states can be directly measured by current vs. bias-voltage characteristics recorded with the tip positioned above a specific point of the nanotube [46] (Fig. 7b). STM and spectroscopy are powerful in correlating microscopic structures with electronic properties in solid state systems, and this is certainly the case for nanotubes. Excellent agreement is found with the main theoretical predictions. That is, arm-chair SWNTs are metallic with a finite density of states at the Fermi level, and semiconducting tubes exhibit energy gaps with zero density of states inside the gap. As expected, the energy gaps of semiconducting SWNTs scale with $1/d$ where d is the diameter of the nanotube. STM studies have also probed interesting quantum phenomena associated with the finite lengths of SWNTs. Venema et al. observed electron standing waves along the axis of short nanotubes by direct STM imaging. The electron density oscillates periodically along the nanotube with wavelength $\approx 2L/n$ (L is the tube length, n the integer). This is a quantum confinement effect as electrons behave like 'particles-in-a-box' with the box being a 1D wire in this case. Odom et al. observed single electron charging effects for electron tunneling from an STM tip to short nanotubes deposited on substrates [47].

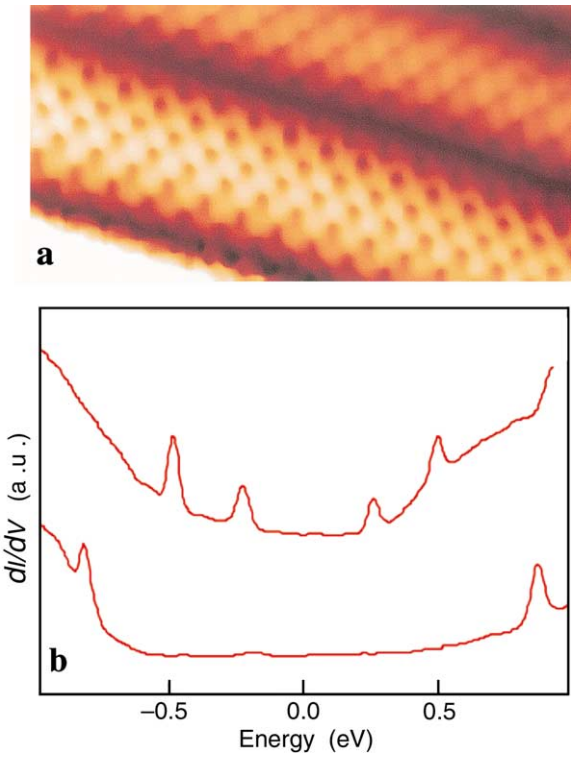

Fig. 7. Probing the real-space atomic structures of SWNTs and correlating structures with electronic properties (courtesy of Dr. C. Lieber). (a) Atomically resolved (dots) STM image of a (12,−2) semiconducting tube (center region between the two darker lines) in a bundle. The dots are associated with the atomic corrugations. (b) Local density of states $(\mathrm{d}I/\mathrm{d}V)/(I/V)$ for a metallic (bottom curve) and semiconducting (top curve) SWNT respectively. The two curves are shifted artificially for clarity. For the semiconducting nanotube (top curve), the density of state in the energy range of −0.2 to 0.2 eV is zero, corresponding to a semiconducting band gap. For the metallic nanotube (bottom curve), the density of states is non-zero at all energies without a band gap. Density of states is defined as the number of electronic states as a function of electronic energy.

4.2. Electron transport in nanotubes

Integrating individual nanotubes into addressable structures is important to elucidate the electron transport properties of nanotubes. Dekker and coworkers made electrical contacts to individual SWNTs grown by laser ablation by depositing SWNTs from liquid suspensions onto predefined electrodes [48]. McEuen and coworkers used AFM to locate SWNTs deposited on a substrate and then placed metal electrodes to contact the nanotubes [49–51]. Our group developed a growth and integration method to contact SWNTs grown from patterned catalyst islands. Large numbers of individually addressable nanotubes are obtained this way (Fig. 8a) [17,31,32,52–58].

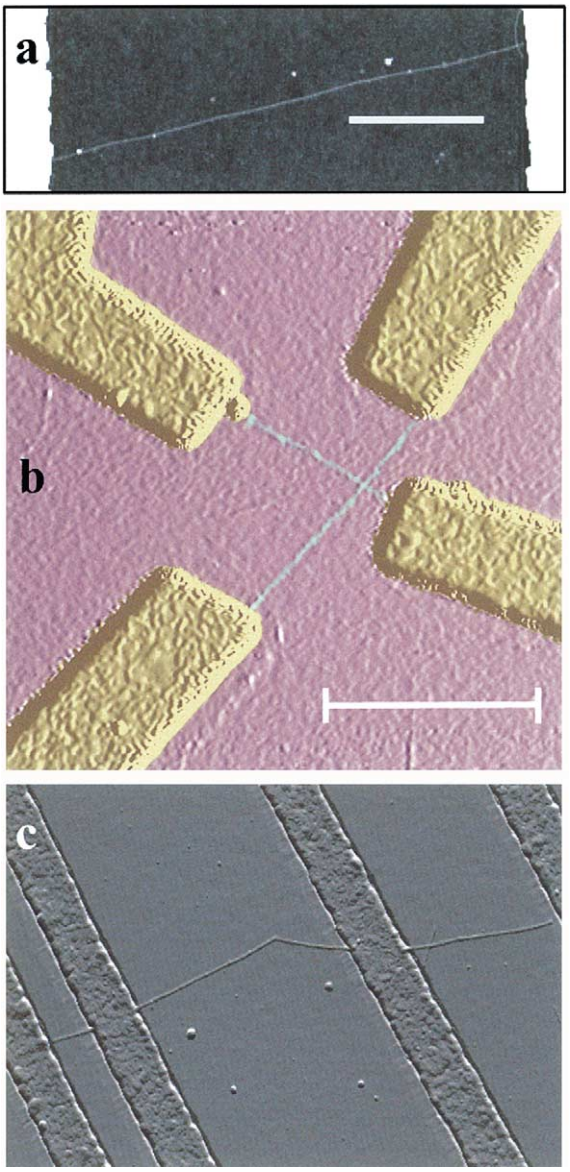

Fig. 8. Connecting SWNTs to the macroscopic world for electrical measurements. (a) AFM image of a SWNT contacted by metal electrodes (bright regions at the left and right of the image). (b) AFM image of two crossing nanotubes each connected to two metal electrodes (courtesy of Dr. P. McEuen). (c) AFM image of a nanotube heterojunction formed by a metallic tube connected to a semiconducting tube (courtesy of Drs. C. Dekker and Z. Yao).

Complex SWNT electrical devices have also been obtained by various approaches. These include intra-tube heterojunctions containing sharp kinks at the junctions [59] (Fig. 8c), SWNT crosses on substrates [57,60] (Fig. 8b) and cross-structures of suspended SWNTs [61].

The ability to connect to nanotubes from the macroscopic world has allowed the investigation of electrical transport properties of individual nanotubes. Generally, a SWNT is identified to be metallic when its room temperature electrical conductance is insensitive to gate voltages applied by an electrode hundred of nanometers away from the tube. The role of the gate voltage is to electrostatically change the chemical potential or Fermi energy of the nanotube. For a metallic tube, the shift in Fermi energy does not significantly change the density of states at the Fermi level. Therefore no significant change in the conductance is expected. An intriguing question has been under what conditions metallic SWNTs behave as ballistic wires. For a metallic SWNT, the Fermi level crosses two energy bands. Therefore, two channels and four electronic states (due to spin up and down degeneracy) should contribute to transport. In the absence of electron scattering and ideal electrical contacts to the nanotube, the conductance of the system should be $4e^2/h = 2G_0$ [62], where $G_0 = 2e^2/h$ is the conductance quantum. That is, each channel should contribute G_0 to the conductance of the system. The corresponding resistance for ballistic transport in a metallic SWNT should be 6.45 kΩ, one half of the resistance quantum $R_Q = h/2e^2$.

Tans [48] and Bockrath [49] carried out the earliest transport measurements of individual metallic SWNTs. These nanotube samples have high resistance on the order of megaohms mainly due to poor metal–tube contacts. Interestingly, nanotubes were found to act as quantum wires. Quantum phenomena observed in these samples include single-electron charging and resonance tunneling through discrete energy states of nanotubes arising from quantum confinement along the length of the tubes [48,49]. Single-electron charging or Coulomb blockade [63] occurs when two conditions are met by a small metallic dot (in this case a tube) connected to two electrodes. The first is that the connections are weak characterized by contact resistance larger than R_Q. The second is that the dot is sufficiently small, therefore the capacitance is

small and the energy needed for adding an electron to the system e^2/C is larger than thermal energy K_BT. The capacitance of a nanotube scales linearly with the inverse of its length. For a micron long nanotube, the single-electron charging energy is sufficiently high for the Coulomb blockade to be observed at liquid helium temperature 4.2 K [48,49]. In the Coulomb blockade regime, transport occurs via individual electrons. Discrete energy levels exist for electrons in a nanotube with finite length, the physics of which is well described by the particle-in-a-box picture with the box being a 1D wire with finite length. When a discrete energy state is aligned with the Fermi level of the system, resonance tunneling occurs [48,49]. Nanotubes are ideal systems to study quantum effects at relatively high temperatures due to their small size, relatively large Coulomb charging energy and energy level spacing for sub-micron long nanotubes.

Single electron charging related phenomena are observed in SWNT samples with high contact resistance. With improved metal–tube contacts, the intrinsic electrical properties of nanotubes can be elucidated. Low contact resistance has been obtained by the growth and integration approach involving titanium electrodes evaporated onto SWNTs [52]. Metallic SWNTs with several microns length between electrodes exhibit two-terminal resistance on the order of tens to hundreds of kΩ. The resistance of a 3 μm long SWNT can be as low as 12 kΩ (Fig. 9a). The linear resistance of the sample decreases as the temperature is decreased, and a slight upturn is observed below 30 K in the resistance vs. temperature curve. Coulomb blockade is not observed because the contact resistance is less than R_Q. The decrease of resistance as temperature decreases is due to reduced phonon scattering at low temperatures [64,65]. The upturn in resistance at low temperature is believed to be due to electron localization [64,65] in 1D systems. Localization is essentially a quantum interference phenomenon that the electron wave function decays exponentially from a point due to a random potential distribution caused by disorder. Localization effects have also been observed by Avouris and coworkers in SWNT rings [66].

Yao and Dekker obtained low resistance metallic SWNT samples by placing SWNTs on top of

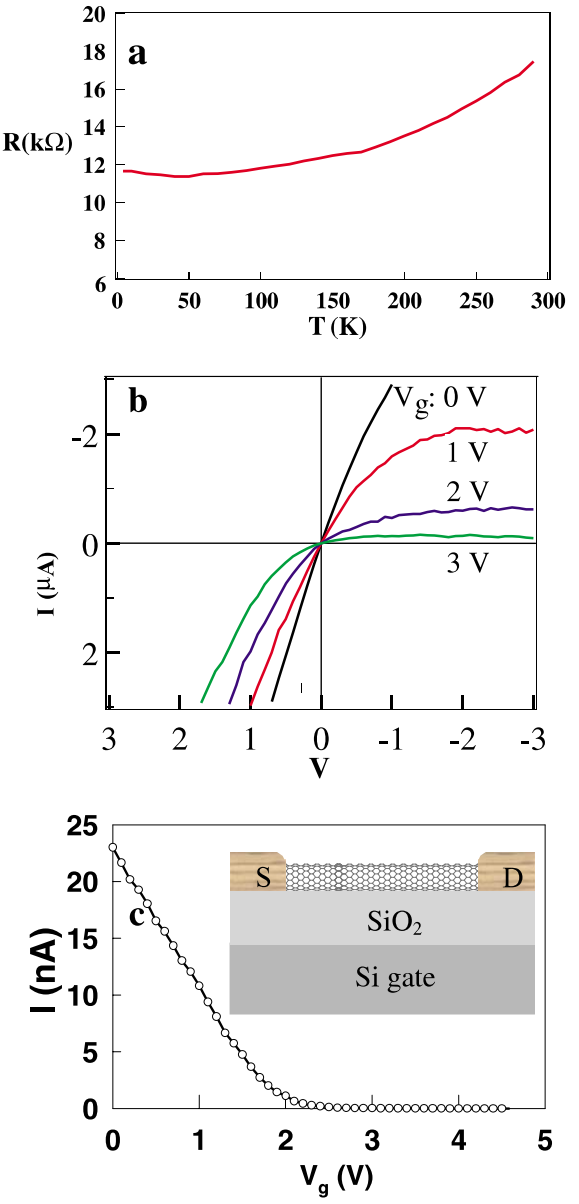

Fig. 9. Electrical properties of individual SWNTs. (a) Resistance as a function of temperature for a metallic SWNT contacted by two Ti electrodes. (b) *I–V* curves for a semiconducting SWNT under various gate voltages V_g. The gate voltage is applied to the sample substrate as illustrated in the inset below. (c) *I* vs. V_g characteristics for the nanotube. The inset shows the schematic sample configuration. The metal-contacted nanotube device with source (S) and drain (D) electrodes is fabricated on a 500 nm thick silicon oxide surface. The silicon substrate underneath the silicon oxide is highly doped and electrically conducting. A gate voltage can be applied to this substrate to capacitively couple to the nanotube.

flat gold electrodes and measured a resistance on the order of 15 kΩ [67]. Bachtold and coworkers used electrostatic AFM to map out the voltage drop across metallic SWNTs and found that the voltage drop along the length of the nanotube is very small [68]. These results all point to ballistic transport with minimum electron scattering in metallic SWNTs.

Tans et al. [69], Martel et al. [70] and Zhou et al. [54] carried out measurements of individual semiconducting SWNTs. These nanotubes exhibit transistor behavior at room temperature, that is, their conductance can be changed dramatically (by orders of magnitude) by gate voltages (Fig. 9b). The nanotubes appeared to be doped with holes as p-type. Positive gate voltages caused the Fermi level shifting away from the valence band into the band gap, depleted the holes and turned the system into insulating states. p-type transistor behavior was observed consistently in semiconducting SWNTs by a number of groups. Hole doping of SWNTs is attributed to adsorbed oxygen [71]. With good metal–tube contacts, low resistance semiconducting SWNT samples on the order of hundreds of kiloohms were obtained by Zhou et al. [54]. The transconductance (ratio of current change over gate-voltage change) of these semiconducting tube samples can be up to ~200 nA/V [54], two orders of magnitude higher than measured in high resistance samples. The high transconductance is a direct result of low sample resistance, since high currents can be transported through the system at relatively low bias voltages. This result is important since high transconductance and voltage gain is essential to the performance of transistors.

McEuen and coworkers studied the electrical properties of crosses of SWNTs [60]. Electron transport from metallic to metallic, metallic to semiconducting, and semiconducting to semiconducting tubes were investigated. The conductance of the metal–metal tube junction was found to be ~0.1 e^2/h, suggesting appreciable electron scattering at the crosses. Metallic and semiconducting tubes were found to form Schottky junctions at the crosses. A Schottky junction is typically formed at the interface between a bulk semiconductor and a pure metal. The difference in workfunction between the two materials causes energy band bending in the semiconductor side. Characteristic of a Schottky junction is rectifying behavior in the current vs. voltage curves [60]. Current flows across the junction only when the metal side is negatively biased. Tombler et al. studied SWNT crosses and used scanning probes as gates to identify the metallic or semiconducting nature of the crossing nanotubes [57].

Chico et al. proposed theoretically that by joining a metallic and semiconducting SWNT with topological defects, such as pentagons and heptagons, novel intramolecular devices can be obtained [72]. Yao et al. investigated intra-tube devices experimentally and observed a sharp kink on an individual SWNT (Fig. 8c) [59]. Electron transport across the kink exhibited rectifying behavior (Fig. 10). The system was suggested to contain a metallic tube joining a semiconducting tube with a Schottky junction formed at the kink. This result demonstrated that extremely small electrical devices are obtainable on an individual molecular wire.

4.3. Chemical doping

Chemical doping effects to the electrical properties of SWNTs have been investigated by several groups. SWNT doping with electron withdrawing

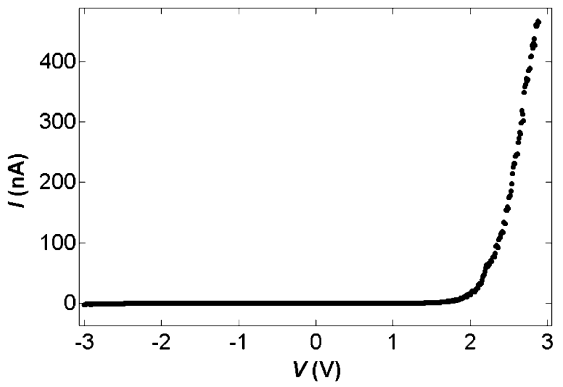

Fig. 10. SWNT heterojunction as intra-molecular rectifier: the world's smallest rectifying junction. The rectifying current vs. voltage characteristics was observed with a SWNT containing a sharp kink in the structure (Fig. 8c).

(Br_2, I_2) and donating species (K, Cs) were first carried out with bulk SWNT mats by Lee et al. and Grigorian et al. [73,74]. Bundles of SWNTs were also studied [75,76]. With bulk mats, chemical doping can lead to orders of magnitude reduction in the resistance of bulk SWNT materials due to the increase in the average of hole or electron carriers in the nanotubes. The doping species absorb on to nanotube surfaces and intercalate into the empty space of bundles of SWNTs [73,74].

It is necessary to investigate individual SWNTs since doping effects in metallic and semiconducting SWNTs can be drastically different. Bockrath et al. carried out potassium doping of a semiconducting SWNT at room temperature. A transition from p-type to n-type was observed as K atoms absorb onto the outer surface of the nanotube and donate electrons to the tube [76]. Similar phenomenon was observed by Kong et al. [77]. Fig. 11a shows the evolution of the conductance as a function of time during K-doping for a diameter ~2.5 nm and length = 0.4 μm SWNT contacted by Ti electrodes. The conductance decreased dramatically by five orders of magnitude and then recovered. This corresponds to the nanotube evolving from p-type to intrinsic and then to n-type semiconducting states under progressive K-doping.

More can be learned about K-doping of single tubes by characterizing the doped nanotubes at low temperatures. Temperature dependent measurements of K-doped SWNTs reveal Coulomb blockade [63] oscillations at high temperatures up to 160 K (Fig. 11b). The Coulomb oscillation peaks in gate voltage (V_g) is periodic and evenly spaced at $\Delta V_g \sim 0.45$ V in regime I of Fig. 11b, where each peak corresponds to charging and transporting one electron through the system. In regime II, the oscillations are periodic with $\Delta V_g \sim 0.45$ V at high temperatures but some of the peaks split into doublets at low temperatures ($T < 110$ K). In regime III, periodic oscillations are observed only at $T < 90$ K with a small period of $\Delta V_g \sim 0.15$ V. These peaks show no splitting down to 20 K. The change of ΔV_g by ~0.45 V causes one electron addition or removal from the dot, the gate capacitance is therefore $C_g = e/\Delta V_g = 0.35$ aF. The total capacitance of the system is estimated to be $C_\Sigma = 3.72$ aF, corresponding to a charging energy of $U = e^2/C_\Sigma = 43$ meV. For charging energy $U \sim 50$ meV, the size of the quantum dot seen in regime I appears smaller than the tube length $L = 0.4$ μm between the edges of metal electrodes. The dot in regime I has an effective length of $L_{eff} \sim 0.1$–0.15 μm, about one third of the actual geometry of the nanotube. This phenomenon is attributed by an inhomogeneous K-doping profile along the nanotube, as a result of the randomness of K-evaporation onto the sample. That is, an inhomogeneous effect can lead to a high temperature SET due to the formation of a single quantum dot with its size smaller than the geometrical tube length. This can occur when the two barriers for the dot are located within the length of the tube while the rest of the system is well coupled to the metal contacts. This suggests that to obtain high temperature nanotube SETs reliably, it is desired to obtain samples with 10–50 nm tube lengths and have great chemical homogeneity along the lengths.

Single-electron transistors operating at room temperatures have been pursued actively with Si and metal systems [78–82]. Nanotubes are potential candidates for high performance SETs. With nanotubes, room temperature single-electron charging will require a tube 'dot' with length on the order of 10–50 nm, so that charging energy can be $U \geqslant 100$ meV $\sim 4 K_B T$ (300 K). Room temperature nanotube SETs could be realized in the near future.

4.4. Nanotube electromechanical properties

The question of how mechanical deformation affects the electrical properties of carbon nanotubes has been under theoretical and experimental studies due to the potential application of nanotubes for nanoscale electro-mechanical (NEMs) devices. The effects of mechanical deformation to the electrical properties of nanotubes were studied theoretically by several groups. Nardelli and coworkers modeled the bending of an arm-chair metallic SWNT and calculated the electrical conductance vs. bending angle [83–85]. The nanotube conductance was found to change only slightly under small bending angles. Rochefort et al. carried out simulations of nanotube bending and found that at larger bending angles ~45°, the electrical conductance of a metallic SWNT can be lowered by up to

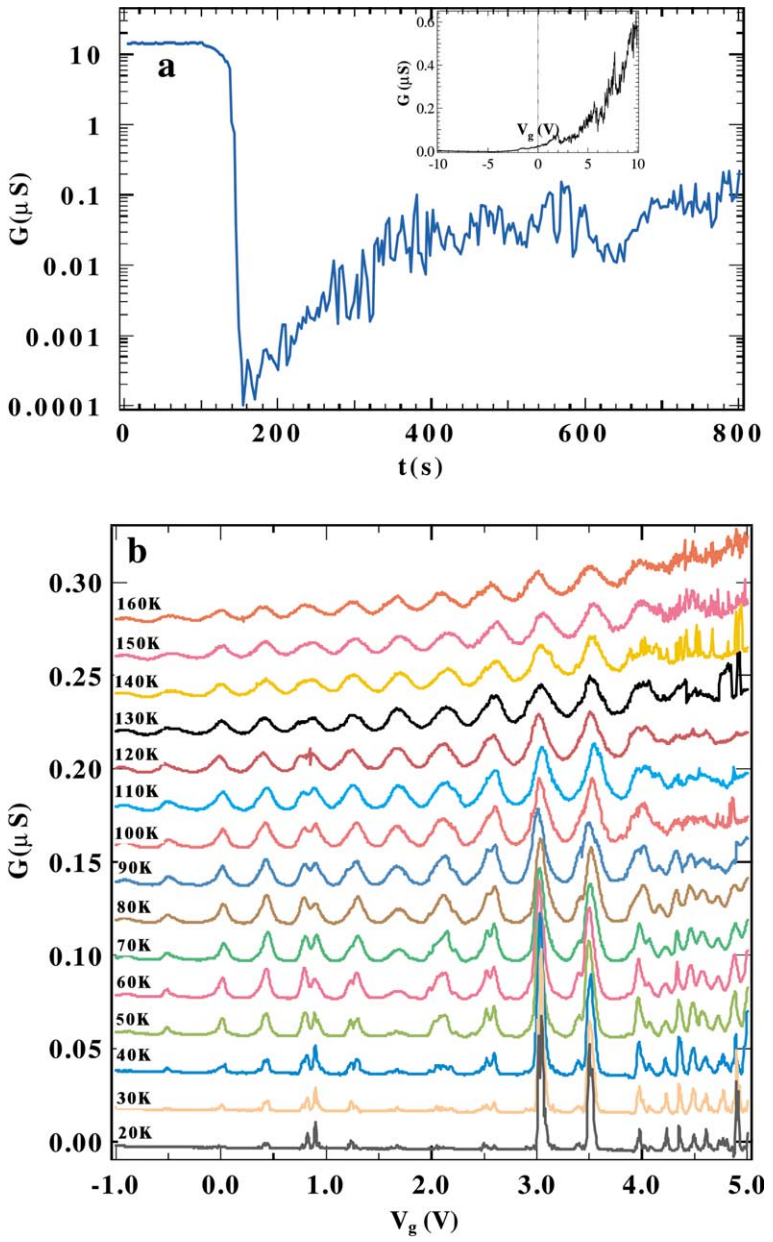

Fig. 11. Elucidating how chemical doping affects the electrical properties of individual SWNTs. (a) Conductance vs. time for a semiconducting SWNT during K doping. The drastic conductance decrease to a nearly insulating state followed by a recovery corresponds to transitions from a p-type (hole rich) to intrinsic to n-type (electron rich) semicondutor, due to electron donation from adsorbed K atoms. Inset: conductance vs. V_g curve at room temperature showing n-type behavior after K-doping. (b) Conductance vs. V_g curves for the doped SWNT at various temperatures showing Coulomb oscillations corresponding to single-electron charging effect. The K-doped nanotube behaves as a single-electron transistor functioning at relatively high temperatures.

10-fold. The conductance decrease was attributed to a σ–π hybridization effect, i.e., some sp^3 bonding characteristics developed at the bent due to increased curvature under high bending angles

[84,85]. The sp^3 atomic structure causes the electrons to be localized and is responsible for the reduced nanotube conductance.

Experimental investigation of the electromechanical properties of nanotubes can be carried out with suspended nanotubes, as shown by Tombler et al. [58]. A nanotube can be grown from patterned catalyst sites across pre-fabricated trenches on SiO_2/Si substrates [58]. This leads to an individual SWNT that is partially suspended over the trenches (Fig. 12a). The suspended part of the nanotube can be manipulated with an AFM tip, while the resistance of the sample is being monitored (Fig. 12b). The nanotube conductance decreases each time the AFM tip pushes the nanotube down, but recovers as the tip retracts (Fig. 12c). The full reversibility of the nanotube electrical conductance upon tip retraction suggests that the metal–tube contacts are not affected each time when the tip deflects the suspended part of the nanotube. The observed change in sample conductance is entirely due to the mechanical deformation of the SWNT caused by the pushing tip.

The conductance is found to decrease by a factor of 2 at $\sim 5^\circ$ bending angle (strain $\sim 0.3\%$), but decreases more dramatically by two orders of magnitude at a bending angle $\sim 14^\circ$ (strain $\sim 3\%$, Fig. 12d) [58]. Wu and coworkers have carried out order-N non-orthogonal tight-binding molecular-dynamics simulations of a tip deflecting a metallic (5,5) SWNT, with the tip modeled by a short and stiff (5,5) SWNT cap [58,86]. At relatively small bending angles, the nanotube is found to retain sp^2 bonding throughout its structure, but exhibits significant bond distortion for the atoms in the region near the tip. As tip-pushing and bending proceed, the nanotube structure progressively evolves and larger structural changes occur in the nanotube region in the vicinity of the tip. At a 15° bending angle, the average number of bonds per atom in this region is found to increase to ~ 3.6, suggesting the appearance of sp^3-bonded atoms (marked in red in Fig. 12e). This causes a significant decrease in the local π-electron density as revealed by electronic structure calculations. Since the π-electrons are delocalized and responsible for electrical conduction, a drastic reduction in the π-electron density is responsible for the significant decrease in conductance. Simulations find that the large local sp^3 deformation is highly energetic, and its appearance is entirely due to the forcing tip. The structure is found to fully reverse to sp^2 upon moving the tip away in the simulation. The combined experimental and theoretical study leads to an in-depth understanding of nanotube electromechanical properties, and suggests that SWNTs could serve as reversible electro-mechanical transducers that are potentially useful for NEMs devices.

5. Surface science in nanotubes

5.1. Metal–nanotube interactions

The interactions between nanotubes and various metals are important to low resistance ohmic contacts to nanotubes and other issues such as forming metal or superconducting nanowires on nanotube templates [87–89]. Experimental and theoretical investigations of the interactions between metals and various carbon materials have been carried out previously. It is known that in three-dimensional bulk materials, different metals exhibit different interactions with carbon. The ability for transition metals to bond with carbon atoms increases with the number of unfilled d-orbitals. Metals such as Al, Au and Pd have no d-vacancies and negligible affinity for carbon. Metals with few d-vacancies such as Ni, Fe and Co exhibit finite solubility for carbon in certain temperature ranges. 3d and 4d metals with many d-vacancies such as Ti and Nb can form strong chemical bonds with carbon and thus highly stable carbide compounds. It is generally believed that the interactions between deposited metals and a graphite basal plane are weak [90–99]. The interactions are suggested to be through van der Waals forces and do not involve chemical bond formations between the metal and carbon atoms in the graphite basal plane. For C_{60} [100–102], it has been shown that certain metals interact much more strongly with C_{60} than graphite including Ti and Ni [100,102]. Deposition of Ti on C_{60} can lead to the formation of Ti–C carbide bonds as revealed by X-ray photoelectron spectroscopy [100].

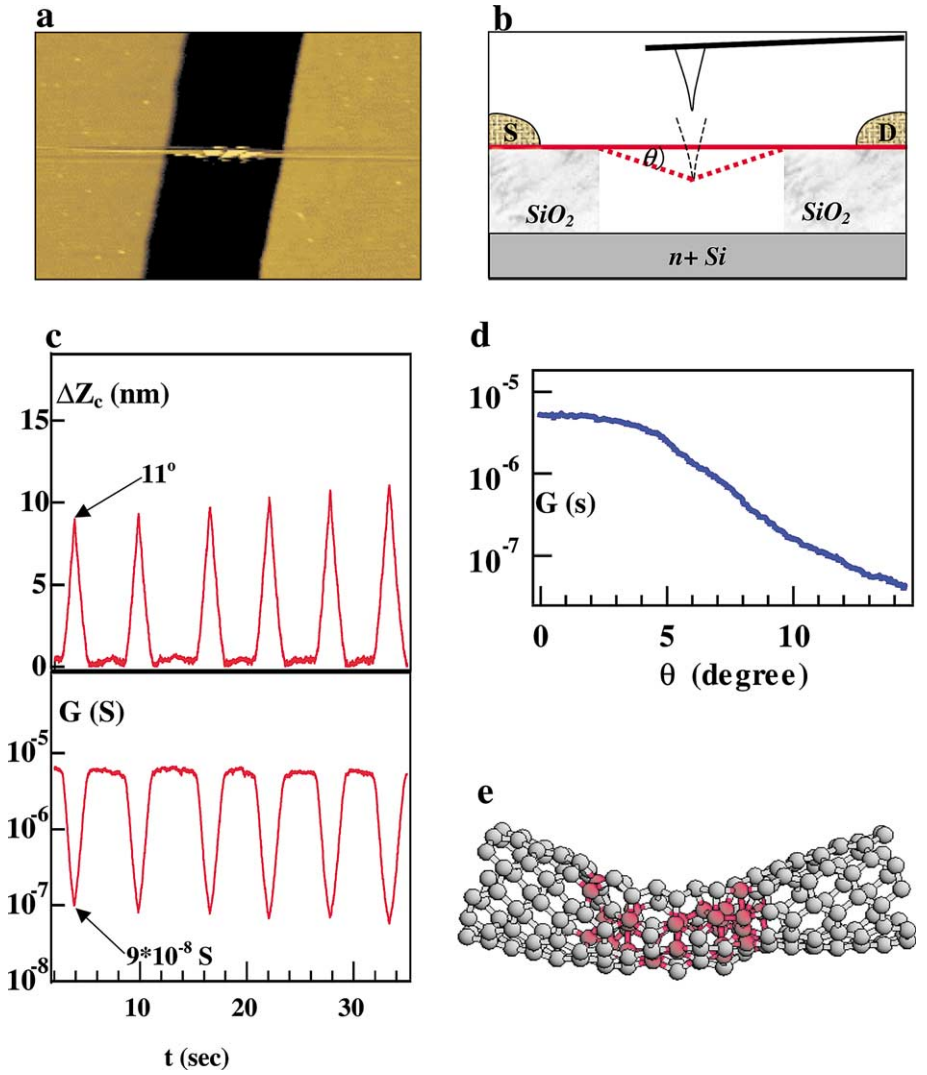

Fig. 12. Elucidating how mechanical deformation affects the electrical properties of SWNTs: electromechanical properties. (a) AFM image of a suspended SWNT over a trench. (b) Experimental scheme for measuring the electromechanical property of the nanotube. The suspended nanotube is pushed downwards by an AFM tip, while the deflection of the cantilever and the conductance of the nanotube sample across the source (S) and drain (D) electrodes are monitored. (c) Upper panel: cantilever deflection (ΔZ_c) vs. time during repeated pushing-down of the suspended nanotube by the AFM tip. The cantilever deflection signal can be used to compute the vertical deflection and bending angle (θ) of the nanotube. Lower panel: Conductance (G, in unit of Ω^{-1}) of the nanotube vs. time recorded simultaneously as the deflection signal. (d) Nanotube conductance vs. bending angle obtained by analyzing the data in (c). (e) Atomic configuration revealed by molecular dynamics simulations (MD) at a bending angle of 15° manipulated by a simulated tip. The red atoms are highlighted because they are bonded to four other atoms (sp^3-like bonding) instead of three atoms as in the unperturbed form of the nanotube. Such structural distortion leads to energy barriers to electron transport and is mainly responsible for the reduced electrical conductance of the nanotube system.

A nanotube differs from a graphene sheet in that the cylindrical sidewall of a nanotube is curved and is in a non-planar sp^2 bonding configuration. A nanotube differs from C_{60} in dimensionality, radius and that C_{60} contains pentagons in its structure, whereas the sidewall of a nanotube

contains exclusively hexagons. C_{60} therefore is expected to be more reactive with metals than a nanotube because of the pentagons in the structure. A recent theoretical study by Menon et al. shed some light into metal–tube interactions [103]. They used a tight-binding molecular-dynamics method to calculate bonding configurations of Ni with the sidewall atoms on a SWNT, and compared the results with Ni bonding on a graphene sheet. Covalent bonding characteristics of Ni (on certain sites) with carbon atoms on the nanotube were identified from the calculations. The interaction was found to be stronger than ionic-like (charge transfer) bonding with a graphene sheet. The strong Ni-SWNT interaction was attributed to curvature-induced rehybridization of carbon sp^2 orbitals with the Ni d-orbital [103].

An experimental investigation of metal–tube interaction was carried out recently by Zhang et al. by studying the structures of various metals formed on suspended SWNTs deposited by electron beam evaporation [104]. 5 nm of Ti, Ni, Pd, Au, Al, and Pb are evaporated to coat suspended SWNTs and drastically different coating results are observed (Fig. 13). Ti forms continuous nanowires on suspended SWNTs (Fig. 13a). Ni and Pd form quasi-continuous and uniform coatings on SWNTs (Fig. 13b and c respectively), with the wire structures occasionally disconnected along the lengths. Au, Al, and Pb deposited on the nanotubes form disconnected crystalline particles, leaving sections of the nanotubes free of metal coating (Fig. 13d, e and f respectively). The Au particles decorating SWNTs are up to $\sim$60 nm wide, much larger than the deposited film thickness. This indicates that Au atoms deposited on the tubes have migrated and merged together to form large particles.

The continuous and uniform Ti coating on nanotubes suggests a high nucleation density and strong Ti–SWNT interaction. On the contrary, the Au and Al coatings are highly discontinuous with a very low nucleation density due to weak Au, Al–SWNT interactions. A low Au-tube binding energy points to a low activation barrier for adatom diffusion. Rapid motion of Au atoms on the nanotube sidewall can cause the atoms or even small clusters to merge into isolated large particles [98]. Ti atoms deposited on nanotubes exhibit the highest condensation/sticking coefficient among Ni and other metals. The Ti–SWNT interaction should be stronger than that for Ni–SWNT and could involve covalent bonding due to the high affinity of Ti for carbide formation and the curvature induced rehybridization effect. The intimate Ti–SWNT interaction and the fact that Ti–C is highly conducting are consistent with the result that low resistance ohmic electrical contacts to individual SWNTs can be reliably made by depositing Ti electrodes onto nanotubes [52]. It was found previously that Ti also makes ohmic contacts to doped diamonds. In this case, as deposited Ti forms carbide bonds with the very surface of diamond, and ohmic contacts are obtained by thermal annealing that leads to a layer of carbide at the Ti–diamond interface [105].

5.2. Interactions with small molecules: nanotube chemical sensors

How molecules interact with carbon nanotubes and affect their physical properties is of fundamental interest, and may have important implications to their applications. The electrical properties of metallic SWNTs are relatively insensitive to their chemical environment and interactions with other species. For an example, potassium doping of a metallic SWNT does not affect its conductance significantly [106], because the band shift due to charge-transfer interactions does not change the density of states at the Fermi level for a metallic tube. Semiconducting SWNTs, on the other hand, are very sensitive to K-doping, and can change from p-type to n-type accompanied by orders of magnitude change in conductance as discussed earlier. Semiconducting SWNTs are also very sensitive to gas molecule adsorption, exhibiting significant changes in their electrical conductance.

Colins et al. [71] have studied molecular oxygen adsorption on carbon nanotubes. The electrical properties of nanotubes are found to be highly sensitive to oxygen adsorption effects. In a vacuum chamber, the conductance of bulk SWNTs increases when oxygen is introduced into the system and recovers when vacuum is restored. Full desorption of oxygen can occur when heating the

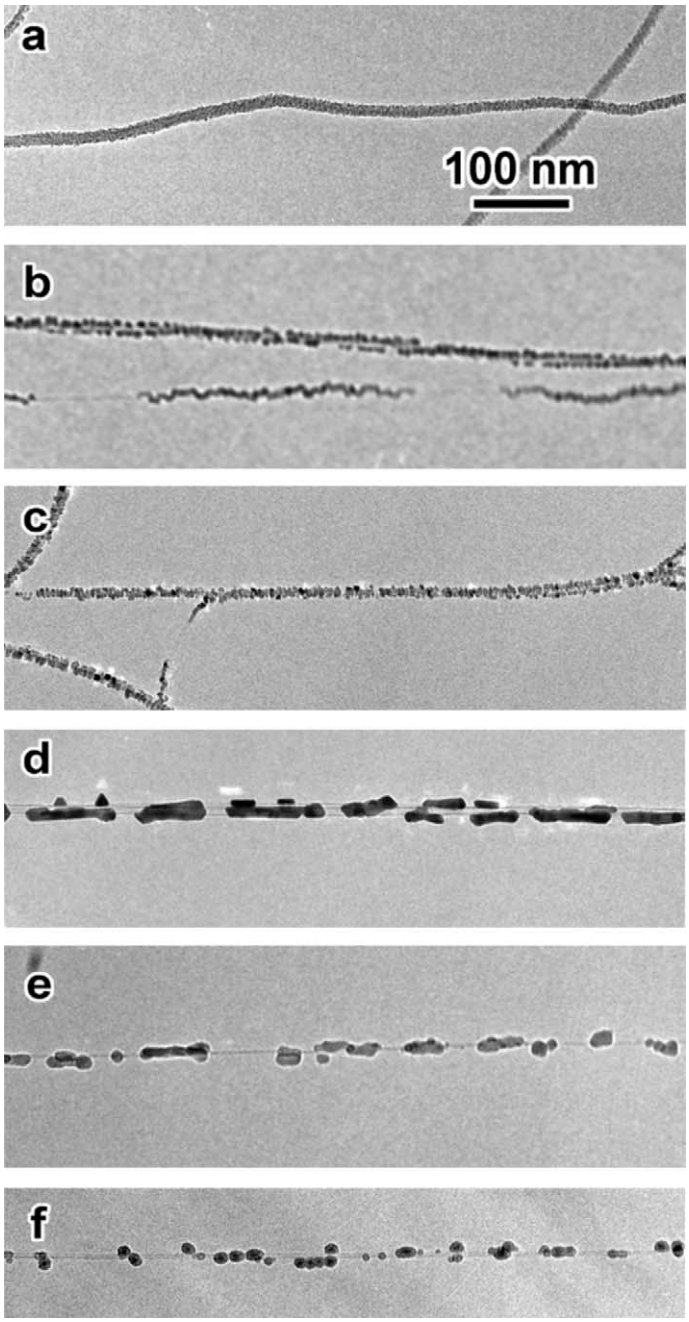

Fig. 13. TEM study of metal–SWNT interactions. The images show the structures of various types of metal deposited onto suspended SWNTs. (a) 5 nm Ti coating on a suspended SWNT. Clearly, Ti atoms deposit uniformly on the SWNT. (b–f) Structures of 5 nm Ni, Pd, Fe, Au, Al and Pb coatings respectively on suspended SWNTs. These metals tend to form discrete particles of various sizes when deposited on SWNTs due to weak metal–tube interactions.

nanotubes to high temperatures in vacuum. Cohen's group carried out density-functional theory (DFT) calculations on oxygen–SWNT complexes and found that oxygen adsorbs on a nanotube with a binding energy of approximately 0.25 eV [107]. An oxygen molecule withdraws about 0.1 electron from the nanotube, causing hole-doping to the nanotube.

Kong et al. found that nanotubes can be used for miniature chemical sensors to detect small concentrations of gas molecules with high sensitivity at room temperature [55]. Chemical sensors based on individual or ensembles of SWNT can detect chemicals such as nitrous oxide (NO_2) and ammonia (NH_3) [55]. For a semiconducting single-wall nanotube exposed to 200 ppm of NO_2, it was found that the electrical conductance can increase by up to three orders of magnitude in a few seconds (Fig. 14a). On the other hand, exposure to 2% NH_3 caused the conductance to decrease by up to two orders of magnitude (Fig. 14b). As a general comparison, conventional solid state sensors for NO_2 and NH_3 typically operate at temperatures over 400 °C, and conducting polymers provide only limited sensitivity. Sensors made from SWNT have high sensitivity and a fast response time at room temperature, which are important advantages for sensing applications.

DFT calculations carried out by Cho and coworkers have revealed that an NO_2 molecule can bind to a semiconducting SWNT with a binding energy of ~0.9 eV (18.4 kcal/mol) [55]. This suggests that the nature of the molecule–tube interaction is strong physisorption and approaching the chemisorption regime. The oxidizing NO_2 molecule withdraws about one-tenth of an electron charge from the nanotube. The charge transfer leads to increased hole carriers and enhanced conductance for the p-type nanotube. The interaction between NH_3 and a SWNT is physisorption in nature. NH_3 is a Lewis base that can donate a small amount of electrons to nanotubes and therefore reduce the hole-carriers.

Modification of nanotubes by chemical or physical means should represent a viable way to enable the development of highly sensitive and selective chemical sensors useful for practical applications. For an example, semiconducting SWNTs coated

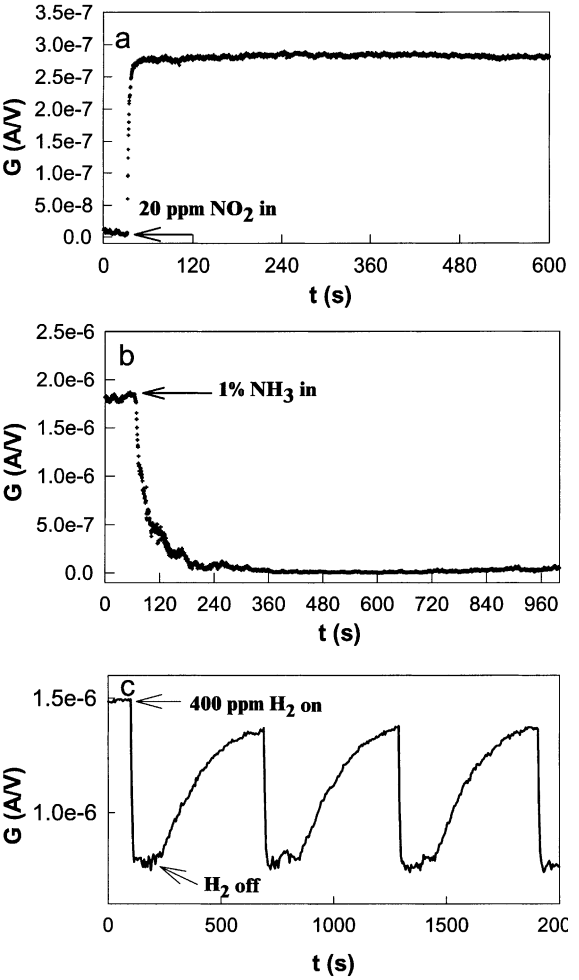

Fig. 14. Elucidating the interactions between molecules and SWNTs and exploring carbon nanotubes for advanced miniature chemical sensors. (a) Conductance response of an individual semiconducting SWNT to 200 ppm of NO_2 in argon. (b) Conductance response of an individual SWNT to 1% NH_3 in argon. (c) Conductance of a Pd-decorated semiconducting SWNT vs. time in a flow of air with 400 ppm of H_2 on and off over several cycles. These results illustrate the potential of nanotube based chemical sensors.

with a non-continuous thin layer of palladium metal become extremely sensitive to molecular hydrogen. The conductance of a palladium-coated semiconducting single-wall nanotube decreases rapidly upon exposure to a flow of air mixed with 400 ppm of hydrogen, and reverses when the hydrogen flow is turned off (Fig. 14c). This clearly shows that palladium modified SWNTs are excellent

hydrogen sensors with fast response, good sensitivity and reversibility under ambient conditions. The mechanism can be understood by considering the interactions between H_2 and the Pd–SWNT system. It is well established that at room temperature, hydrogen molecules dissociate into atomic hydrogen on Pd surfaces [108]. The resulting atomic hydrogen dissolves into Pd with high solubility and consequently lowers the work function (energy required to remove an electron from the Fermi level) of Pd [108]. This causes electron transfer from Pd to SWNTs, which lowers the hole-carriers in the nanotube and thus its conductance.

The Pd-modified SWNT sensors are readily reversible when the hydrogen flow is stopped, as the dissolved atomic hydrogen in Pd combines with oxygen in air and leaves Pd–SWNT system in the form of water [108]. These features and mechanisms bear certain resemblance to conventional hydrogen sensors based on semiconductor field-effect transistors with Pd gates, as pioneered by Lundstrom [109].

6. Conclusion and outlook

Carbon nanotubes present significant opportunities to basic science and nanotechnology, and pose significant challenge for future work in this field. The approach of direct growth of nanowires into ordered structures on surfaces is a promising route to approach nanoscale problems and create novel molecular-scale devices with advanced electrical, electromechanical and chemical functions. Gaining further control in nanotube growth will continue to open new possibilities in basic science and real-world applications. It is an ultimate goal for growth to produce defect-free nanotubes at the ton level by simple and efficient methods, gain control over the nanotube chirality and diameter, and be able to direct the growth of a semiconducting or metallic nanowire from and to any desired sites.

Acknowledgements

We are grateful to Drs. C. Lieber, S. Iijima, P. McEuen, C. Dekker, Z. Yao, S. Xie and Z. Ren for providing some of the data shown in this article. Work carried out at Stanford were in collaboration with Professors C. Quate, S. Fan, S. Y. Wu, C. S. Jayanthi, K. Cho, S. Manalis and C. Marcus, supported by National Science Foundation, DARPA/ONR, a Packard Fellowship, a Terman Fellowship, Semiconductor Research Corporation/Motorola Co., Semiconductor Research Corporation/Semetech, ABB Group Ltd., the National Nanofabrication Users Network at Stanford, Stanford Center for Materials Research, a Packard Fellowship for Science and Engineering, a Terman Fellowship, the Camile Henry-Dreyfus Foundation and the American Chemical Society.

References

[1] H.W. Kroto, J.R. Heath, S.C. O'Brien, R.F. Curl, R.E. Smalley, C_{60}: Buckminsterfullerene, Nature 318 (1985) 162–163.
[2] S. Iijima, Helical microtubules of graphitic carbon, Nature 354 (1991) 56–58.
[3] S. Iijima, T. Ichihashi, Single-shell carbon nanotubes of 1-nm diameter, Nature 363 (1993) 603–605.
[4] B.I. Yakobson, R.E. Smalley, Fullerene nanotubes: $C_{1,000,000}$ and beyond, Am. Sci. 85 (1997) 324–337.
[5] M.S. Dresselhaus, G. Dresselhaus, P.C. Eklund, Science of Fullerenes and Carbon Nanotubes, Academic Press, San Diego, 1996.
[6] N. Hamada, S. Sawada, A. Oshiyama, New one-dimensional conductors: graphitic microtubules, Phys. Rev. Lett. 68 (1992) 1579–1581.
[7] M.S. Dresselhaus, G. Dresselhaus, P. Avouris (Eds.), Carbon Nanotubes, Springer, Berlin, 2001.
[8] T.W. Ebbesen, P.M. Ajayan, Large-scale synthesis of carbon nanotubes, Nature 358 (1992) 220–222.
[9] D.S. Bethune, C.H. Kiang, M. DeVries, G. Gorman, R. Savoy, J. Vazquez, R. Beyers, Cobalt-catalysed growth of carbon nanotubes with single-atomic-layer walls, Nature 363 (1993) 605–607.
[10] A. Thess, R. Lee, P. Nikolaev, H. Dai, P. Petit, J. Robert, C. Xu, Y. Lee, S. Kim, A. Rinzler, D. Colbert, G. Scuseria, D. Tomanek, J. Fischer, R. Smalley, Crystalline ropes of metallic carbon nanotubes, Science 273 (1996) 483–487.
[11] C. Journet, W. Maser, P. Bernier, A. Loiseau, M. Delachapelle, S. Lefrant, P. Deniard, R. Lee, J. Fischer, Large-scale production of single-walled carbon nanotubes by the electric-arc technique, Nature 388 (1997) 756–758.
[12] G.G. Tibbetts, M.G. Devour, E.J. Rodda, An adsorption-diffusion isotherm and its application to the growth of carbon filaments on iron catalyst particles, Carbon 25 (1987) 367–375.

[13] G.G. Tibbetts, Why are carbon filaments tubular? J. Cryst. Growth 66 (1984) 632–638.
[14] R.T.K. Baker, Catalytic growth of carbon filaments, Carbon 27 (1989) 315–323.
[15] H.G. Tennent, Hyperion Catalysis International, Inc. US patent #4663230, USA, 1987.
[16] M. Endo, Grow carbon fibers in the vapor phase, Chemtech 18 (1988) 568–576.
[17] H. Dai, Growth and characterization of carbon nanotubes, in: M.S. Dresselhaus, G. Dresselhaus, P. Avouris (Eds.), Carbon Nanotubes, Springer, Berlin, 2001, pp. 29–53.
[18] J. Kong, A.M. Cassell, H. Dai, Chemical vapor deposition of methane for single-walled carbon nanotubes, Chem. Phys. Lett. 292 (1998) 567–574.
[19] J. Kong, H. Soh, A. Cassell, C.F. Quate, H. Dai, Synthesis of individual single-walled carbon nanotubes on paterned silicon wafers, Nature 395 (1998) 878.
[20] A. Cassell, J. Raymakers, J. Kong, H. Dai, Large scale single-walled nanotubes by CVD synthesis, J. Phys. Chem. 103 (1999) 6484–6492.
[21] M. Su, B. Zheng, J. Liu, A scalable CVD method for the synthesis of single-walled carbon nanotubes with high catalyst productivity, Chem. Phys. Lett. 322 (2000) 321–326.
[22] E. Flahaut, A. Govindaraj, A. Peigney, C. Laurent, C.N. Rao, Synthesis of single-walled carbon nanotubes using binary (Fe, Co, Ni) alloy nanoparticles prepared in situ by the reduction of oxide solid solutions, Chem. Phys. Lett. 300 (1999) 236–242.
[23] J.-F. Colomer, C. Stephan, S. Lefrant, G. Tendeloo, I. Willems, Z. Kónya, A. Fonseca, C. Laurent, J. Nagy, Large-scale synthesis of single-wall carbon nanotubes by catalytic chemical vapor deposition (CCVD) method, Chem. Phys. Lett. 317 (2000) 83–89.
[24] J. Hafner, M. Bronikowski, B. Azamian, P. Nikolaev, D. Colbert, R. Smalley, Catalytic growth of single-wall carbon nanotubes from metal particles, Chem. Phys. Lett. 296 (1998) 195–202.
[25] H. Cheng, F. Li, G. Su, H. Pan, M. Dresselhaus, Large-scale and low-cost synthesis of single-walled carbon nanotubes by the catalytic pyrolysis of hydrocarbons, Appl. Phys. Lett. 72 (1998) 3282–3284.
[26] P. Nikolaev, M. Bronikowski, R. Bradley, F. Rohmund, D. Colbert, K. Smith, R. Smalley, Gas-phase catalytic growth of single-walled carbon nanotubes from carbon monoxide, Chem. Phys. Lett. 313 (1999) 91–97.
[27] W.Z. Li, S. Xie, L. Qian, B. Chang, B. Zou, W. Zhou, R. Zhao, G. Wang, Large-scale synthesis of aligned carbon nanotubes, Science 274 (1996) 1701–1703.
[28] Z. Pan, S.S. Xie, B. Chang, C. Wang, Very long carbon nanotubes, Nature 394 (1998) 631–632.
[29] Z.F. Ren, Z.P. Huang, J.W. Xu, J.H. Wang, Synthesis of large arrays of well-aligned carbon nanotubes on glass, Science 282 (1998) 1105–1107.
[30] S. Fan, M. Chapline, N. Franklin, T. Tombler, A. Cassell, H. Dai, Self-oriented regular arrays of carbon nanotubes and their field emission properties, Science 283 (1999) 512–514.
[31] H. Dai, J. Kong, C. Zhou, N. Franklin, T. Tombler, A. Cassell, S. Fan, M. Chapline, Controlled chemical routes to nanotube architectures, physics and devices, J. Phys. Chem. 103 (1999) 11246–11255.
[32] H. Dai, Controlling nanotube growth, Phys. World 13 (2000) 43–47.
[33] A. Cassell, N. Franklin, T. Tombler, E. Chan, J. Han, H. Dai, Directed growth of free-standing single-walled carbon nanotubes, J. Am. Chem. Soc. 121 (1999) 7975–7976.
[34] N. Franklin, H. Dai, An enhance chemical vapor deposition method to extensive single-walled nanotube networks with directionality, Adv. Mater. 12 (2000) 890.
[35] H. Dai, J. Hafner, A. Rinzler, D. Colbert, R. Smalley, Nanotubes for nanoprobes, Nature 384 (1996) 147–150.
[36] S. Wong, E. Joselevich, A. Woolley, C. Cheung, C. Lieber, Covalently functionalized nanotubes as nanometrel-sized probes in chemistry and biology, Nature 394 (1998) 52–55.
[37] S. Wong, J. Harper, M. Lansbury, C.M. Lieber, Carbon nanotube tips: high-resolution probes for imaging biological systems, J. Am. Chem. Soc. 120 (1998) 603–604.
[38] H. Dai, N. Franklin, J. Han, Exploiting the properties of carbon nanotubes for nanolithography, Appl. Phys. Lett. 73 (1998) 1508–1510.
[39] S. Wong, A. Wooley, E. Joselevich, C. Lieber, Functionalization of carbon nanotube AFM probes using tip-activated gases, Chem. Phys. Lett. 306 (1999) 219–225.
[40] S. Wong, A. Woolley, E. Joselevich, C. Cheung, C. Lieber, Covalently functionalized single-walled carbon nanotube probe tips for chemical force microscopy, J. Am. Chem. Soc. 120 (1998) 8557–8558.
[41] J. Hafner, C. Cheung, C. Lieber, Growth of nanotubes for probe microscopy tips, Nature 398 (1999) 761–762.
[42] J. Hafner, C. Cheung, C.M. Lieber, Direct growth of single-walled carbon nanotube scanning probe microscopy tips, J. Am. Chem. Soc. 121 (1999) 9750–9751.
[43] E.B. Cooper, S. Manalis, H. Fang, H. Dai, K. Matsumoto, S. Minne, T. Hunt, C.F. Quate, Terabit-per-square-inch data storage with the atomic force microscope, Appl. Phys. Lett. 29 (1999) 3566–3568.
[44] T. Odom, J. Huang, P. Kim, C.M. Lieber, Atomic structure and electronic properties of single-walled carbon nanotubes, Nature 391 (1998) 62–64.
[45] J.W.G. Wildoer, L.C. Venema, A.G. Rinzler, R.E. Smalley, C. Dekker, Electronic structure of atomically resolved carbon nanotubes, Nature 391 (1997) 59.
[46] M. Ouyang, J.-L. Huang, C.M. Lieber, Harvard University, unpublished results.
[47] T.W. Odom, J.L. Huang, P. Kim, C.M. Lieber, Structure and electronic properties of carbon nanotubes, J. Phys. Chem. 104 (2000) 2794–2809.

[48] S.J. Tans, M. Devoret, H. Dai, A. Thess, R. Smalley, L. Geerligs, C. Dekker, Individual single-wall carbon nanotubes as quantum wires, Nature 386 (1997) 474–477.
[49] M. Bockrath, D. Cobden, P. McEuen, N. Chopra, A. Zettl, A. Thess, R. Smalley, Single-electron transport in ropes of carbon nanotubes, Science 275 (1997) 1922–1925.
[50] D. Cobden, M. Bockrath, N. Chopra, A. Zettle, P. McEuen, A. Rinzler, R. Smalley, Spin splitting and even–odd effects in carbon nanotubes, Phys. Rev. Lett. 81 (1998) 681–684.
[51] J. Nygard, D.H. Cobden, M. Bockrath, P.L. McEuen, P.E. Lindelof, Electrical transport measurements on single-walled carbon nanotubes, Appl. Phys. A 69 (1999) 297–304.
[52] H. Soh et al., Integrated nanotube circuits: controlled growth and ohmic contacting of single-walled carbon nanotubes, Appl. Phys. Lett. 75 (1999) 627–629.
[53] A. Morpurgo, J. Kong, C. Marcus, H. Dai, Gate controlled superconducting proximity effect in nanotubes, Science 286 (1999) 263–265.
[54] C. Zhou, J. Kong, H. Dai, Electrical measurements of individual semiconducting single-walled nanotubes of various diameters, Appl. Phys. Lett. 76 (1999) 1597.
[55] J. Kong, N. Franklin, C. Zhou, M. Chapline, S. Peng, K. Cho, H. Dai, Nanotube molecular wires as chemical sensors, Science 287 (2000) 622–625.
[56] C. Zhou, J. Kong, H. Dai, Intrinsic electrical properties of single-walled carbon nanotubes with small band gaps, Phys. Rev. Lett. 84 (2000) 5604.
[57] T. Tombler, C. Zhou, J. Kong, H. Dai, Gating individual nanotubes and crosses with scanning probes, Appl. Phys. Lett. 76 (2000) 2412.
[58] T. Tombler, C. Zhou, L. Alexeyev, J. Kong, H. Dai, L. Liu, C. Jayanthi, M. Tang, S. Wu, Reversible nanotube electro-mechanical characteristics under local probe manipulation, Nature 405 (2000) 769.
[59] Z. Yao, H.W.C. Postma, L. Balents, C. Dekker, Carbon nanotube intramolecular junctions, Nature 402 (1999) 273–276.
[60] M.S. Fuhrer, J. Nygård, L. Shih, M. Forero, Y. Yoon, M. Mazzoni, H. Joon, J. Choi, S. Louie, A. Zettl, P. McEuen, Crossed nanotube junctions, Science 288 (2000) 494–497.
[61] T. Rueckes, K. Kim, E. Joselevich, G. Tseng, C. Cheung, C. Lieber, Carbon nanotube-based nonvolatile random access memory for molecular computing, Science 289 (2000) 94–97.
[62] C.T. White, T.N. Todorov, Carbon nanotubes as long ballistic conductors, Nature 393 (1998) 240.
[63] H. Grabert, M.H. Devoret (Eds.), Single Charge Tunneling, Plenum Press, New York, 1992.
[64] J.E. Fischer, H. Dai, A. Thess, R. Lee, N. Hanjani, D. De Haas, R. Smalley, Metallic resistivity in crystalline ropes of single-wall carbon nanotubes, Phy. Rev. B-Condens. Matter 55 (1997) R4921–R4924.
[65] C.L. Kane, E. Mele, R. Lee, J. Fischer, P. Petit, H. Dai, A. Thess, R. Smalley, A. Verschueren, A. Tans, C. Dekker, Temperature dependent resistivity of single wall carbon nanotubes, Euro. Phys. Lett. 6 (1998) 683–688.
[66] H.R. Shea, R. Martel, M. Avouris, Electrical transport in rings of single-wall nanotubes: one-dimensional localization, Phys. Rev. Lett. 84 (2000) 4441.
[67] Z. Yao, C. Dekker, personal communication.
[68] A. Bachtold, M. Fuhrer, S. Plyasunov, M. Forero, E. Anderson, A. Zettl, P. McEuen, Scanned probe microscopy of electronic transport in carbon nanotubes, Phys. Rev. Lett. 84 (2000) 6082–6085.
[69] S. Tans, A. Verschueren, C. Dekker, Room-temperature transistor based on a single carbon nanotube, Nature 393 (1998) 49–52.
[70] R. Martel, T. Schmidt, H.R. Shea, T. Hertel, P. Avouris, Single- and multi-wall carbon nanotube field-effect transistors, Appl. Phys. Lett. 73 (1998) 2447–2449.
[71] P.G. Collins, K. Bradley, M. Ishigami, A. Zettl, Extreme oxygen sensitivity of electronic properties of carbon nanotubes, Science 287 (2000) 1801–1804.
[72] L. Chico, V.H. Crespi, L.X. Benedict, S.G. Louie, M.L. Cohen, Pure carbon nanoscale devices—nanotube heterojunctions, Phys. Rev. Lett. 76 (1996) 971–974.
[73] R.S. Lee, H.J. Kim, J.E. Fischer, A. Thess, R.E. Smalley, Conductivity enhancement in single-wall carbon nanotube bundles doped with K and Br, Nature 388 (1997) 255–257.
[74] L. Grigorian, K. Williams, S. Fang, G. Sumanasekera, A. Loper, E. Dickey, S. Pennycook, P. Eklund, Reversible intercalation of charged iodine chains into carbon nanotube ropes, Phys. Rev. Lett. 80 (1998) 5560–5563.
[75] R.S. Lee, H. Kim, J. Fischer, J. Lefebvre, M. Radosavljevi, J. Hone, A. Johnson, Transport properties of a potassium-doped single-wall carbon nanotube rope, Phys. Rev. B 61 (2000) 4526–4529.
[76] M. Bockrath, J. Hone, A. Zettl, P. McEuen, A. Rinzler, R. Smalley, Chemical doping of individual semiconducting carbon-nanotube ropes, Phys. Rev. B 61 (2000) R10606–R10608.
[77] J. Kong, C. Zhou, E. Yenilmez, H. Dai, Alkaline metal doped n-type semiconducting nanotubes as quantum dots, Appl. Phys. Lett. 77 (2000) 3977.
[78] H. Ishikuro, T. Fujii, T. Saraya, G. Hashiguchi, T. Hiramoto, T. Ikoma, Coulomb blockade oscillations at room temperature in a Si quantum wire metal-oxide-semiconductor field-effect transistor fabricated by anisotropic etching on a silicon-on-insulator substrate, Appl. Phys. Lett. 68 (1996) 3585–3587.
[79] H. Ishikuro, T. Hiramoto, Quantum mechanical effects in silicon quantum dot in a single-electron transistor, Appl. Phys. Lett. 71 (1997) 3691–3693.
[80] L. Zhuang, L. Guo, S.Y. Chou, Silicon single-electron quantum-dot transistor switch operating at room temperature, Appl. Phys. Lett. 72 (1998) 1205–1207.
[81] K. Matsumoto, M. Ishii, K. Segawa, Y. Oka, B. Vartanian, J. Harris, Room temperature operation of a single

electron transistor made by the scanning tunneling microscope nanooxidation process for the TiO_x/Ti system, Appl. Phys. Lett. 68 (1996) 34–36.
[82] Y.A. Pashkin, Y. Nakamura, J.S. Tsai, Room-temperature Al single-electron transistor made by electron-beam lithography, Appl. Phys. Lett. 76 (2000) 2256–2258.
[83] M. Nardelli, J. Bernholc, Mechanical deformations and coherent transport in carbon nanotubes, Phys. Rev. B 60 (1998) R16338–16341.
[84] A. Rochefort, D. Salahub, P. Avouris, The effect of structural distortions on the electronic structure of carbon nanotubes, Chem. Phys. Lett. 297 (1998) 45–50.
[85] A. Rochefort, F. Lesage, D. Salhub, P. Avouris, Conductance of distorted carbon nanotubes, 1999 xxx.lanl.gov/cond-mat/9904083.
[86] L. Liu, C. Jayanthi, M. Tang, S. Wu, T. Tombler, C. Zhou, L. Alexeyev, J. Kong, H. Dai, Controllable reversibility of an transition of a sp^2 to sp^3 single wall nanotube under the manipulation of an AFM tip: a nanoscale electromechanical switch? Phys. Rev. Lett. 84 (2000) 4950.
[87] H. Dai, E.W. Wong, Y.Z. Lu, F. Shoushan, C.M. Lieber, Synthesis and characterization of carbide nanorods, Nature 375 (1995) 769–772.
[88] W.Q. Han, S.S. Fan, Q.Q. Li, Y.D. Hu, Synthesis of gallium nitride nanorods through a carbon nanotube-confined reaction, Science 277 (1997) 1287–1289.
[89] A. Bezryadin, C.N. Lau, M. Tinkham, Quantum suppression of superconductivity in ultrathin nanowires, Nature 404 (2000) 971.
[90] Q. Ma, A. Rosenberg, Interaction of Ti with the (0001) surface of highly oriented pyrolytic graphite, Phys. Rev. B 60 (1999) 2827–2832.
[91] M. Baumer, J. Libuda, H. Freund, The temperature dependent growth mode of nickel on the basal plane of graphite, Surf. Sci. 327 (1995) 321–329.
[92] P. Kruger, A. Rakotomahevitra, J. Parlebas, C. Demangeat, Magnetism of epitaxial 3d-transition-metal monolayer on graphite, Phys. Rev. B (1998) 5276–5280.
[93] S.S. Peng, B.R. Cooper, Y.G. Hao, Modeling of adsorption of iron impurities at the surface of graphite, Philo. Mag. 73 (1996) 611–617.
[94] D. Tomanek, W. Zhong, Palladium–graphite interaction potentials based on first-principles calculations, Phys. Rev. B 43 (1991) 12623–12625.
[95] Q. Ma, R. Rosenberg, Interaction of Al clusters with the (0001) surface of highly oriented pyrolytic graphite, Surf. Sci. 391 (1997) L1224–1229.
[96] I. Moulett, Ab-initio molecular-dynamics study of the interaction of aluminum clusters on a graphite surface, Surf. Sci. 333 (1995) 697–702.
[97] E. Ganz, K. Sattler, J. Clarke, Scanning tunneling microscopy of Cu, Ag, Au and Al adatoms small clusters, and islands on graphite, Surf. Sci. 219 (1989) 33–67.
[98] L. Barfotti, P. Jensen, A. Hoareau, M. Treilleux, B. Cabaud, A. Perez, F. Aires, Diffusion and aggregation of large antimony and gold clusters deposited on graphite, Surf. Sci. 367 (1996) 276.
[99] J. Arthur, A. Cho, Adsorption and desorption kinetics of Cu and Au on (0001) graphite, Surf. Sci. 36 (1973) 641–660.
[100] T.R. Ohno, Y. Chen, S. Harvey, G. Kroll, J. Weaver, R. Haufler, R. Smalley, C_{60} bonding and energy-level alignment on metal and semiconductor surfaces, Phys. Rev. B 44 (1991) 13747–13755.
[101] V. Vijayakrishnan, A. Santra, R. Seshadri, R. Nagarajan, T. Pradeep, C. Rao, A comparative study of the interaction of nickel clusters with buckministerfullerene C_{60} and graphite, Surf. Sci. 262 (1992) L87–90.
[102] E. Parks, K. Kerns, S.R.B. Winter, Adsorption of C_{60} on nickel clusters at high temperatures, Phys. Rev. B 59 (1999) 13431.
[103] M. Menon, A. Andriotis, G. Froudakis, Curvature dependence of metal catalyst atom interaction with carbon nanotubes walls, Chem. Phys. Lett. 320 (2000) 425–434.
[104] Y. Zhang, N. Franklin, R. Chen, H. Dai, A metal coating study of suspended carbon nanotubes and its implications to metal-tube interactions, Chem. Phys. Lett. 331 (2000) 35–41.
[105] T. Tachibana, B. Williams, J. Glass, Correlation of the electrical properties of metal contacts on diamond films with the chemical nature of the metal–diamond surface. II. Titanium contacts: a carbide forming metal, Phys. Rev. B 45 (1992) 11975–11981.
[106] J. Kong, H. Dai, unpublished results.
[107] S. Jhi, S.G. Louie, M.L. Cohen, Electronic properties of oxidized carbon nanotubes, Phys. Rev. Lett. 85 (2000) 1710.
[108] A. Mandelis, C. Christofides, Physics Chemistry and Technology of Solid State Gas Sensor Devices, Wiley, New York, 1993.
[109] I. Lundstrom, M. Shivaraman, C. Svensson, Chemical reactions on palladium surfaces studied with Pd-MOS structures, Surf. Sci. 64 (1977) 497.